Effect of spin-orbit and on-site Coulomb interactions on the electronic structure and lattice dynamics of uranium monocarbide

U. D. Wdowik,[1] P. Piekarz,[2] D. Legut,[3] and G. Jagło[1]

[1]*Institute of Technology, Pedagogical University, ul. Podchorazych 2, 30-084 Cracow, Poland*

[2]*Institute of Nuclear Physics, Polish Academy of Sciences, ul. Radzikowskiego 152, 31-342 Cracow, Poland*

[3]*IT4Innovations Center, VSB-Technical University of Ostrava, 17.listopadu 15, 708 33 Ostrava, Czech Republic*

(Received 7 April 2016; revised manuscript received 24 May 2016; published 3 August 2016)

Uranium monocarbide, a potential fuel material for the generation IV reactors, is investigated within density functional theory. Its electronic, magnetic, elastic, and phonon properties are analyzed and discussed in terms of spin-orbit interaction and localized versus itinerant behavior of the $5f$ electrons. The localization of the $5f$ states is tuned by varying the local Coulomb repulsion interaction parameter. We demonstrate that the theoretical electronic structure, elastic constants, phonon dispersions, and their densities of states can reproduce accurately the results of x-ray photoemission and bremsstrahlung isochromat measurements as well as inelastic neutron scattering experiments only when the $5f$ states experience the spin-orbit interaction and simultaneously remain partially localized. The partial localization of the $5f$ electrons could be represented by a moderate value of the on-site Coulomb interaction parameter of about 2 eV. The results of the present studies indicate that both strong electron correlations and spin-orbit effects are crucial for realistic theoretical description of the ground-state properties of uranium carbide.

DOI: 10.1103/PhysRevB.94.054303

I. INTRODUCTION

The uranium carbides (monocarbide UC, dicarbide UC_2, and sesquicarbide U_2C_3) have drawn renewed experimental [1–3] and theoretical [4–13] interest which stems from a potential use of these materials as advanced nuclear fuels for the so-called generation IV reactors (including the gas-cooled and sodium-cooled fast reactors) [14,15]. These metallic carbides possess several safety-related advantages over conventional oxide fuels, such as insulating UO_2, which are presently utilized in the nuclear fuel cycle. In particular, they can operate at about 40% of their melting temperature, in contrast to 80% for oxide fuels [16]. They also exhibit higher actinide density, higher thermal conductivity, higher melting point, higher fusion temperature, a better structural stability, and a lower moderation during irradiation compared to the oxide fuels [17]. The majority of these properties have been determined from experiments performed over decades in the last century [18].

Recently, however, the uranium carbides have received considerable theoretical attention which follows from the fundamental point of view as the physics underlying basic properties of uranium carbides, which is not yet fully understood, is governed by the competition between localization and itinerancy of the $5f$ electrons as well as spin-orbit interactions (SOI). Both effects are recognized as dominant factors in determining structural, electronic, magnetic, and dynamical properties of compounds from the U-C system. Also, a better understanding of the behavior of $5f$ electrons remains crucial for description and prediction of the nuclear fuels performance during the in-pile operation as well as for development of modern nuclear fuel materials with desired properties, such as those involving mixed-carbide fuels, like (U, Pu)C. On the other hand, a complexity of the phenomena determining the fundamental properties of the uranium carbides poses a real challenge for theoretical treatment of these compounds within currently well-established first-principles methods such as density functional theory (DFT). Nevertheless, the recent DFT studies that addressed the structural, electronic, magnetic, and elastic properties of UC, UC_2, and U_2C_3 at the ground state [5,8,10–13] have shed a light on how to tackle a partial localization of the $5f$ electron states in those carbides. These investigations employed the DFT+U scheme (with U denoting the effective on-site Coulomb repulsion interaction parameter between the $5f$ states) or the Heyd-Scuseria-Ernzerhof (HSE) screened hybrid potentials to capture the correlated nature of the open $5f$ shell.

Some attempts have also been undertaken to study the lattice dynamics [6] as well as the defect structure of UC [7,9] by using the conventional DFT or DFT+U approaches. Despite these efforts, there are still problems to correctly reproduce the experimentally determined electronic and magnetic properties of UC which remain ambiguous in the light of various theoretical investigations [9,12]. Furthermore, the DFT+U implementation employed to describe dynamics of the UC lattice was unsuccessful too, as the calculated dispersion relations of the optical phonons [6,13] showed large deviations from experiments [19]. No explanation for such a discrepancy has been given to date, either. On the other hand, an accurate description of the high-frequency optical phonons is crucial for predicting the heat transport in actinide materials, as already demonstrated for NpO_2 and UO_2, where optical branches have been shown to contribute about 30% to the thermal conductivity [20,21].

We note that only a few theoretical studies aimed at the description of electronic and elastic properties of UC took into account the spin-orbit interactions [10,22], and the effect of SOI on the phonon dynamics in uranium monocarbide was left highly unexplored. Obviously, in the actinide compounds not only the highly correlated nature of $5f$ states but also the spin-orbit interaction may have an important impact on phonons as well as properties derived from the higher-order derivatives of the total energy (e.g., Raman frequencies) [23]. These motivated us to revisit both the electronic structure and lattice

dynamics of UC in the presence of spin-orbit coupling and strong electron correlations in the open $5f$ shell. Here, both effects are treated on an equal footing. We investigate the influence of the localization of the $5f$ electrons of uranium atoms on the electronic and dynamical properties of UC. A degree of localization/itinerancy of the $5f$ electrons is tuned by varying the parameter U, representing the strong local interactions of the Coulomb type. Our theoretical DFT+U investigations supplemented with SOI (DFT+U+SO) show qualitatively distinct band structure and dynamics of phonons from those produced by conventional DFT or DFT+U implementations. The present results obtained within the DFT+U+SO scheme closely correlate with the x-ray photoemission (XPS) and bremsstrahlung isochromat (BIS) spectroscopes [24] as well as the inelastic neutron scattering (INS) experiments [19,25], which seems to validate our findings.

II. METHODOLOGY

Our theoretical studies are based on the spin-polarized DFT method implementing the projector-augmented-wave (PAW) formalism to describe the electron-ion interactions and the generalized gradient approximation parametrized by Pedrew, Burke, and Ernzerhof (GGA-PBE) for the exchange-correlation potential [26,27]. The Kohn-Sham wave functions are expanded into plane waves up to a cutoff energy of 520 eV. The valence electrons of uranium and carbon atoms are represented by configurations of $(6s^2 6p^6 5f^3 6d^1 7s^2)$ and $(2s^2 2p^2)$, respectively. Both the spin-orbit coupling and additional on-site Coulomb repulsion interaction are considered concurrently. The latter are taken into account within the rotationally invariant form of the GGA+U approach [28], where the localized $5f$ electrons experience a spin- and orbital-dependent potential (U) and the exchange interaction J, while the other orbitals are delocalized and treated by the conventional GGA approximation. We control a degree of localization/itinerancy of the $5f$ electrons on uranium atoms by changing the value of U and holding the value of J. The term U is varied from 0 eV for delocalized $5f$ states to 3.5 eV for partially localized ones. The upper limit of U follows from previous theoretical considerations [6,29]. For actinide materials, the exchange parameter J is usually within the range of 0 to 0.7 eV [30], and hence we adopt $J = 0.5$ eV, as already established for UC [10,22].

Uranium carbide holds a stable rocksalt structure (space group $Fm\bar{3}m$, No. 225) within a wide range of temperatures and stoichiometries [3]. Its unit cell contains 8 atoms (4 U and 4 C atoms). Calculations are performed with the $10\times10\times10$ Monkhorst-Pack mesh of $\mathbf{k}$ points, as a function of the Hubbard potential U, with SOI included, and without symmetry constraints imposed on the structures conforming to the $Fm\bar{3}m$ space group. The convergence criteria for the system total energy and residual Hellmann-Feynman (HF) forces are set to 10^{-7} eV and 10^{-5} eV/Å, respectively. The type-I antiferromagnetic order (AFM-I), in which the magnetic moments on the U atoms are aligned within the (100) layer and opposite to the moments of the next (100) layer, is considered as the most energetically favorable over the other antiferromagnetic or ferromagnetic arrangements as well as nonmagnetic configuration [7]. Due to a tendency of the DFT+U to create metastable states in the actinide compounds, an additional analysis of the AFM-I structure is carried out using the controlled symmetry reduction (CSR) method [31]. The multiple local minima on the adiabatic energy surface, being the identification of the metastable states, are not found. The components of the elastic tensor (C_{ij}) are determined from the linear-response method [32].

The dynamical properties of the UC lattice are obtained within the harmonic approximation and the direct method [33], which utilizes the DFT calculated HF forces acting on all atoms in a given supercell. Previously, this method has been applied to other uranium and plutonium compounds [34,35] and successfully verified by the experimental studies [36,37]. Phonons are calculated for the 64-atom supercells, derived from the optimized unit cells, which take into consideration the effects of interaction resulting from the AFM-I order. Such supercells were found to be large enough to avoid contributions from atoms belonging to the periodic images, as confirmed by the elements of the force constant matrices which decay by more than three orders of magnitude at the distances smaller than the boundaries of the supercells. The Brillouin zone integration is performed with the reduced number of $\mathbf{k}$ points ($4\times4\times4$). The nonvanishing HF forces required to construct respective dynamical matrix $\mathbf{D}(\mathbf{k})$ are generated by displacing the symmetry nonequivalent U and C atoms from their equilibrium positions by the amplitude of ±0.02 Å. Hence, for each configuration the total number of the calculated displacements amounts to 4.

The intensities of the phonon modes in one-phonon coherent neutron scattering are directly related to the phonon form factor $F(\mathbf{k}, j)$ taking on the form [33,38]

$$F(\mathbf{k}, j) = \frac{1}{\mathbf{k}^2}\left|\sum_{\mu,i}\frac{\mathbf{k}\cdot\mathbf{e}_i(\mathbf{k}, j;\mu)}{\sqrt{M_\mu}}\right|^2, \tag{1}$$

where M_μ is the mass of the μth atom involved in the j phonon branch at the wave vector $\mathbf{k}$, while $\mathbf{e}_i(\mathbf{k}, j;\mu)$ denotes the polarization vector of the mode $(\mathbf{k}, j)$. We consider relative intensities of the phonon modes which are given with respect to the highest intensity mode (its intensity is taken as 100%). For convenience, the relative intensities of the phonon modes will be denoted by color symbols. Details of the methodology can be found elsewhere [39].

The generalized phonon density of states is evaluated as [40,41]

$$G(E) = \sum_\mu c_\mu \frac{\sigma_\mu}{M_\mu} g_\mu(E) \tag{2}$$

with c_μ, σ_μ, and $g_\mu(E)$ denoting concentration, total neutron scattering cross section, and the partial phonon density of states for the μth atomic species, respectively. The total scattering cross sections for uranium and carbon atoms are $\sigma_{\mathrm{U}} = 8.908$ barns and $\sigma_{\mathrm{C}} = 5.551$ barns [42].

III. RESULTS AND DISCUSSION

A. Electronic structure

In general, an accurate and realistic description of the phonon dynamics in a given system requires a prior insight into its electronic structure as it strongly determines structural features of a material such as the atomic bonding and force constants which in turn affect the system's dynamical properties [43]. Below we present modifications of the electronic and magnetic properties experienced by uranium carbide upon SOI and delocalization/localization of the $5f$ electrons.

In order to see exclusively the effect of SOI on the UC electron structure, we initially treat the $5f$ electronic states as fully delocalized ($U = 0$ eV). Figure 1 compares the resulting band structures simulated with and without inclusion of SOI. The spin-orbit interaction separates the band extending from -5 eV to 6 eV into two well-resolved valence subbands. This separation arises from the splitting of $5f_{5/2}$ and $5f_{7/2}$ states which amounts to 1 eV. The densities of states near and well above the Fermi energy (E_F) are dominated by the U($5f$) states, independently of whether we take the SOI into account or not. The valence and conduction bands also contain a small admixture of U($6d$) states which are superposed over the $5f$ states. Both U($5f$) and U($6d$) states are hybridized with the C($2p$) states, which spread all over the valence and conduction bands. The contribution from the C($2p$) states to the total $D(E)$ is most significant at the bottom of the valence band, i.e., between 5 eV and 1.5 eV below the Fermi level. Additionally, the C($2s$) states form a well-separated band located at 7–10.5 eV below E_F. We note that similar features of the electronic density of states have been reported by Trygg *et al.* [22] who also considered the spin-orbit interaction and fully itinerant $5f$ electrons in the UC compound.

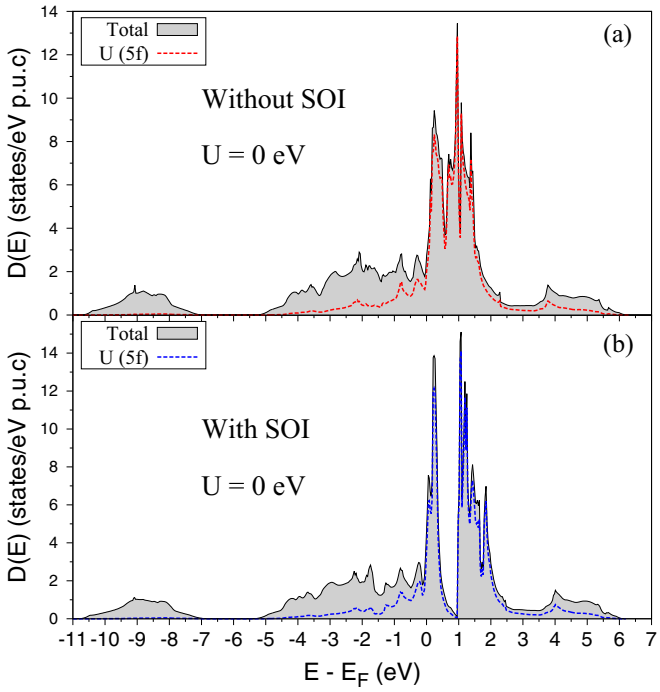

FIG. 1. Total and orbital-projected densities of electron states $D(E)$ for UC with fully itinerant $5f$ electrons ($U = 0$ eV). (a) $D(E)$ with SOI neglected. (b) $D(E)$ with SOI included. Shaded areas and dashed lines represent total and U($5f$) densities of states, respectively. The Fermi level (E_F) is taken as the reference energy.

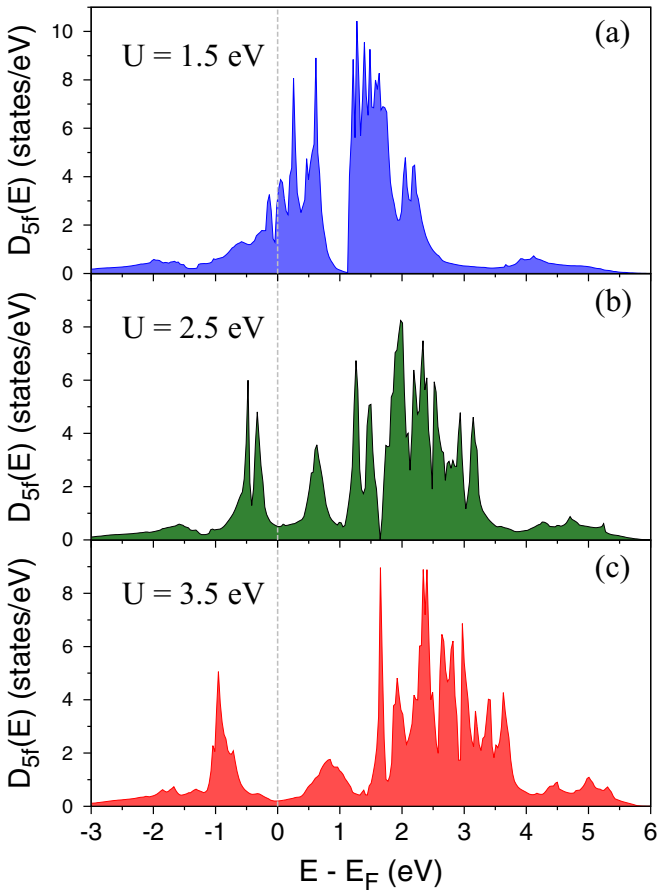

FIG. 2. Dependence of the electron density of states projected onto uranium $5f$ orbitals on the Hubbard potential U in uranium carbide. Partial densities of states with spin-orbit interaction at (a) $U = 1.5$ eV, (b) $U = 2.5$ eV, (c) $U = 3.5$ eV. The Fermi level (E_F) is taken as the reference energy.

Next, we present the evolution of the U($5f$) electron density of states as a function of the Hubbard term U which governs the localization of the $5f$ electrons. In contrast to the previous DFT+U calculations [6] suggesting only a marginal sensitivity of the UC electronic structure to the choice of U, the present DFT+U+SO results, shown in Fig. 2, indicate sizable changes in the electron densities upon increasing the strong on-site Coulomb repulsion. First of all, the parameter U is responsible for the separation of electronic states at the edge of the Fermi level. The energies of the $5f$ electrons below (above) E_F experience downward (upward) energy shift with increased U. Therefore, a small gap separating the $j = 5/2$ and $j = 7/2$ multiplets due to SOI also shifts toward higher energies. This finally leads to the disappearance of that gap for higher values of the U parameter.

The densities of electronic states calculated within the DFT+U+SO scheme can be confronted with those determined by the XPS and BIS experiments [24]. After detailed analysis of the results gained for different Hubbard potentials, we establish $U = 2$ eV as the most suitable value to give the

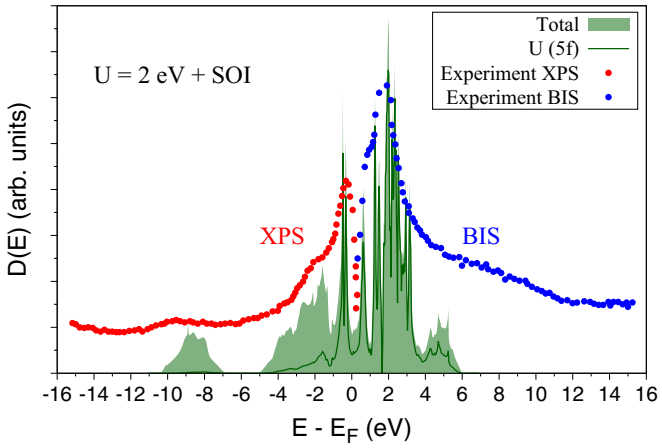

FIG. 3. Comparison of the total and $5f$-orbital projected electron density of states with the BIS and XPS measurements [24] in UC.

closest agreement between the theory and experiment. Figure 3 provides a comparison between the XPS+BIS data and the densities of electronic states determined at $U = 2$ eV. The inclusion of spin-orbit interactions into calculations allows us to better reproduce such features of the valence band XPS spectrum as a single intense peak at the binding energy of about 0.6 eV as well as the two-peak structure of the BIS spectrum appearing in the excited-state region between 1–3 eV. Also, the present DFT+U+SO results seem to follow the experimental observation indicating reduced density of electronic states in the vicinity of the Fermi energy. We mention that all these characteristic features of the experimental spectra could not be reproduced by either DFT or DFT+U approach [6,9].

The increased localization of the $5f$ electrons results in a reduction of the spectral density at the Fermi energy, $N(E_F)$, as depicted in Fig. 4(a). Thus, the calculated electronic specific heat coefficient $\gamma^{\rm cal}$, which is directly related to $N(E_F)$ in the approximation of the free-electron gas model, becomes considerably reduced with localization of the $5f$ electrons. For example, $\gamma^{\rm cal} = 13.6$ mJ K^{-2} mol^{-1} at the limit of itinerant $5f$ states, while $\gamma^{\rm cal} = 1.73$ mJ K^{-2} mol^{-1} at their partial localization ($U = 3.5$ eV). On the other hand, the measured specific heat at low temperatures shows a linear electronic contribution to the low-temperature heat capacity $\gamma^{\rm exp} \sim$ (18–20.3) mJ K^{-2} mol^{-1} [2,17] which corresponds to the electron effective-mass enhancement factor ranging from about 1.4 to about 12 for delocalized and partially localized ($U = 3.5$ eV) $5f$ states, respectively. A close correspondence to the mass enhancement factor of 3.7, determined from the dynamical mean-field theory calculations [10], is found at $U = 1.5$–2.0 eV.

Our spin-polarized calculations indicate that for the fully itinerant $5f$ states, the UC compound is a Pauli paramagnet with negligible value of the total magnetic moment ($M \sim 0.02\,\mu_B$) at the uranium site. Here, the total magnetic moment consists of the spin (M_S) and orbital (M_L) contributions. Our results confirm those previously obtained for UC within the full-potential linear muffin-tin orbital method [22], where the spin-orbit coupling was taken into account and the $5f$ electrons were treated as entirely delocalized. On the other hand, one expects that application of the DFT+U approach to capture

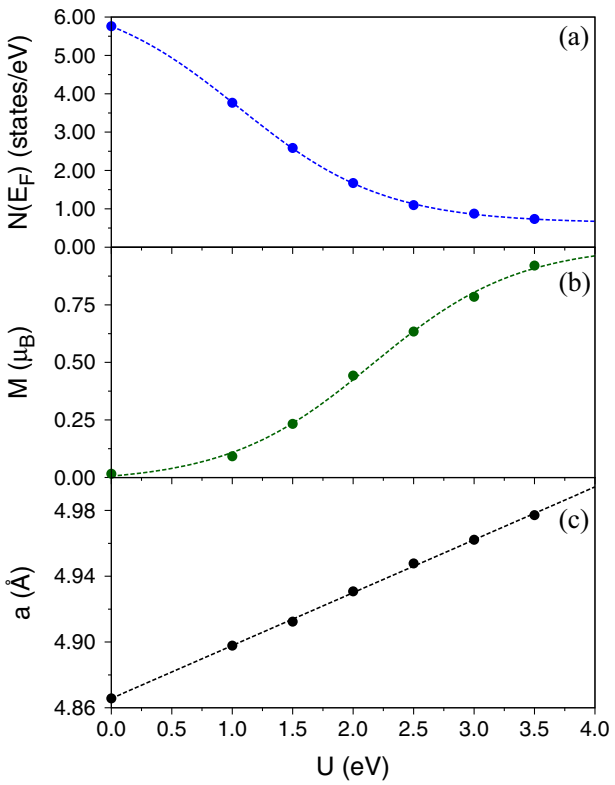

FIG. 4. Influence of the on-site Coulomb interaction represented by Hubbard potential U on (a) density of electron states at the Fermi level $N(E_F)$, (b) absolute value of the total magnetic moment M on uranium atom, (c) lattice constant a in UC.

the correlated nature of the $5f$ states may yield a different magnetic solution from that produced by conventional DFT. This is mainly because the $5f$ states experience the spin- and orbital-dependent potential, which usually tends to enhance the magnetic moment of a system [44]. Such a situation is indeed encountered in UC since we observe an increase of M with increased localization of the $5f$ electrons, in a manner shown in Fig. 4(b). The enhancement of M is due to an increase of both M_S and M_L components upon increased U. Our DFT+U+SO calculations indicate that the orbital component of the moment at the uranium site is larger than, and antiparallel to, the spin component for all considered values of the Hubbard potential U. Moreover, the higher the value of the U parameter, the larger the difference between M_S and M_L. For example, the absolute values of $M_S = 0.60\,\mu_B$ and $M_L = 1.04\,\mu_B$ are found at $U = 2.0$ eV, while they reach $M_S = 0.73\,\mu_B$ and $M_L = 1.66\,\mu_B$ at $U = 3.5$ eV.

The observed reduction of $N(E_F)$ and enlargement of M with increasing localization of the $5f$ wave functions are correlated with a linear increase of the crystal unit cell parameter (a) which is presented in Fig. 4(c). The lattice constant of UC expands by about 2% at $U = 3.5$ eV with respect to that at $U = 0$ eV. The value of 4.96 Å, recommended for the lattice parameter of pure UC (4.8 wt.% C) in equilibrium with higher carbides at room temperature [18], can be achieved for $U = 2$–3 eV. We should mention that the lattice constant of UC strongly depends not only on the sample composition (the total C/U ratio) [45,46] but also on the measurement accuracy,

TABLE I. Calculated and experimental [47,48] elastic constants (C_{ij}) and bulk modulus (B) in UC for selected Hubbard potentials U. The C_{ij} and B are expressed in (GPa). Bulk modulus is derived from the calculated C_{ij} as $B = (C_{11} + 2C_{12})/3$.

U (eV)	C_{11}	C_{12}	C_{44}	B
0.0	389	104	15	199
2.0	316	70	63	152
3.5	348	65	83	159
Exp.	315	77–79	61–65	156–158

the type of heat treatment as well as the presence of nitrogen and oxygen impurities in the UC lattice [17]. Obviously, the increase of a is equivalent to an enlargement of the spacing between uranium atoms. This weakens an overlap of the $5f$ wave functions, i.e., increases a tendency to localization of the $5f$ states and finally promotes the magnetism in UC [7].

B. Elastic properties

The independent components of the elastic tensor in UC remain influenced by the spin-orbit coupling and on-site Coulomb interactions, as indicated in Table I. The UC system with delocalized $5f$ electrons shows on one hand substantially overestimated C_{11}, C_{12}, and bulk modulus B, but on the other hand too low C_{44} in comparison with the experimental values determined at room temperature [47,48]. One can bring the C_{ij} and B to the values reported in experiments by pushing the $5f$ states into partial localization. The behavior of C_{ij} and B versus applied U reflects, however, a complex relation between the electronic structure and bonding properties in UC. A reasonable agreement between the measured and calculated elastic constants is obtained at $U = 2.0$ eV. We have to note that localization of the $5f$ electrons alone, i.e., omission of the SOI, is insufficient to produce components of the UC elastic tensor that correspond well enough to those reported by various experiments [17]. Therefore, the previously applied DFT+U approach [6] was unable to give satisfactory C_{ij} for none of the considered values of the on-site Coulomb repulsion interaction parameter.

Due to the changes in the electronic structure and interatomic distances, arising from both the spin-orbit interaction and partial localization of the $5f$ electrons, the atomic force constants, which govern the phonon dynamics, become modified as well. Figure 5 illustrates behavior of the on-site force constants of the uranium (Φ_U) and carbon (Φ_C) atoms as functions of increased localization of the $5f$ states. Here, we compare Φ_U and Φ_C determined within the DFT+U and DFT+U+SO approaches. An initial softening of the Φ_U and Φ_C calculated with the incorporated SOI appears only at $U < 1$ eV, i.e., when the values of the Hubbard term do not exceed the energy splitting of $5f_{5/2}$ and $5f_{7/2}$ electron states. Such an effect is, of course, not observed for the on-site force constants obtained from the calculations neglecting the SOI that result in the increase of Φ_U and Φ_C with increased localization of the $5f$ electrons. A similar trend becomes also visible for the on-site

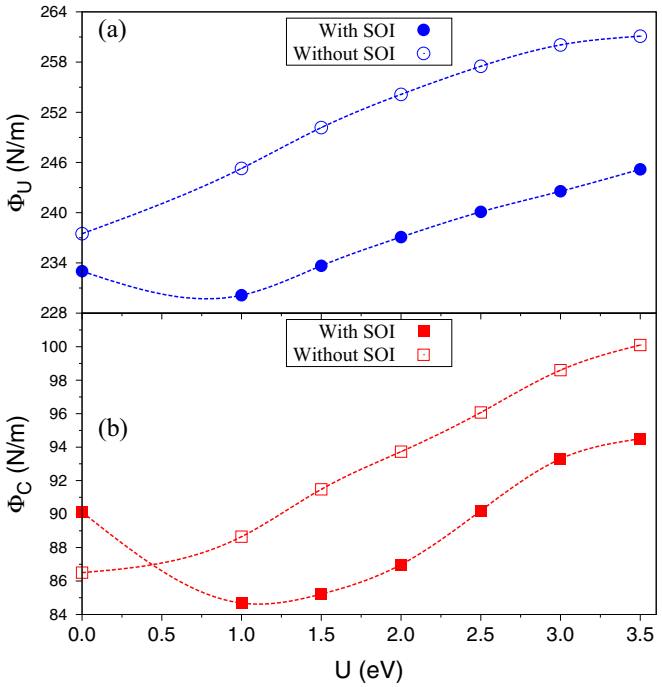

FIG. 5. Influence of the on-site Coulomb interaction represented by Hubbard potential U on the on-site force constants in UC. (a) On-site force constants for uranium atoms (Φ_U), (b) on-site force constants for carbon atoms (Φ_C) determined with the DFT+U (open symbols) and DFT+U+SO (solid symbols) schemes.

force constants given by the DFT+U+SO implementation at $U > 1$ eV, though their values remain lower than those produced by the typical DFT+U approach. In both schemes an enhancement in the force constants can be assigned mostly to the charge redistribution while increasing the Coulomb repulsion on the uranium atoms sites as the more strong localization of the $5f$ electrons prevents the charge flow. The carbon atoms also experience these changes, but indirectly, and their force constants are smaller from those on uranium sites due to significantly smaller atomic mass of carbon compared to uranium. It is worth mentioning that both Φ_U and Φ_C can be additionally affected by the changes in the crystal geometry, i.e., modifications of the U-C bond lengths upon increased localization of the $5f$ states. This effect is, however, negligible in UC since the increase in the U-C interatomic distance over the range of presently considered values of U remains too low ($\sim$1% and $\sim$2% for DFT+U and DFT+U+SO, respectively) to account for such a pronounced enhancement of the on-site force constants.

C. Phonons

Analysis of the phonon dispersion relations calculated for various Hubbard terms U allowed us to establish that the best agreement with the available experimental data can be obtained only when both spin-orbit and the on-site Coulomb iterations with $U \sim 2$ eV are taken into account. A slight underestimation of the theoretical lattice parameter a, determined at $U\sim$2 eV, with respect to the experimental value (0.6%) as well as very small effective magnetic moment

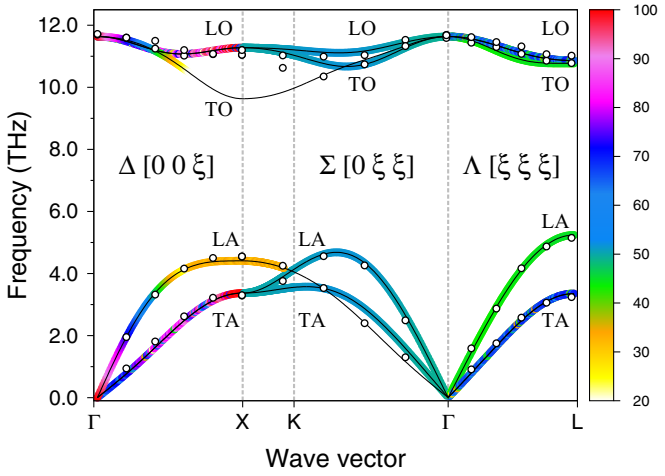

FIG. 6. Dispersion relations of phonons (thin black solid curves) with the overlaid relative intensities of the phonon modes (thick color curves corresponding to the intensity bar) in UC calculated within the DFT+U+SO approach at $U = 2$ eV. The highest intensity mode is taken as a reference (100%). The INS data (open symbols) are adopted from Ref. [19].

M ($\sim 0.5\,\mu_B$) have negligible effect on the phonon energies, as shown by the resulted dispersions of phonons which are compared to those measured by the INS experiments [19] in Fig. 6.

The UC compound is a typical example of a system with a large mass difference of the constituents resulting in a separation of atomic vibrations into a low-frequency phonon band arising mainly from oscillations of heavy uranium atoms, and a high-frequency band constituted by vibrations of light carbon atoms. These bands are well separated by a frequency gap. The acoustic phonon branches (transverse TA and longitudinal LA) belong to the low-frequency band whereas the optical branches (transverse TO and longitudinal LO) form the high-frequency band. In general, the present DFT+U+SO simulations reproduce the experimental TA and LA modes with a high accuracy and confirm that the transverse acoustic phonons remain doubly degenerate along the Γ-X and Γ-L directions, but split along the Γ-K-X direction.

The incorporated SOI together with the Hubbard correction term could remove most of large discrepancies existing between the INS experiments [19] and either the conventional DFT [13] or DFT+U ($U = 3$ eV) [6] results. In general, both approaches produce largely underestimated transverse and longitudinal components of the phonon optical modes which additionally do not follow the course of the experimentally determined branches. Moreover, the previous DFT and DFT+U calculations produced largely dispersive TO and LO branches, contrary to the flat ones measured in the INS experiments. We point out that dispersionless optic branches are characteristic not only for UC, but also for some other rocksalt-structured UX compounds, where $X =$ As, Sb, S, Se, Te [49,50]. In these materials, frequencies of the TO and LO modes are very close to each other. This effect is particularly pronounced for the [0 0 ξ] and [ξ ξ ξ] phonon branches in UC. Only the presence of SOI together with moderate values of Hubbard correction terms, i.e., $U \sim 2$ eV, enabled us to restore degeneracy of the TO branch observed experimentally as well as the course of the measured dispersion curves in the [ξ ξ ξ] direction. Hence, the [ξ ξ ξ] TO branch remains sensitive to both on-site Coulomb and spin-orbit interactions as the increased localization of the 5f electrons ($U > 2$ eV) results in a meaningful softening of this branch and leads to quite large departure from the experimental observations, in a manner similar to that reported in Ref. [6]. On the other hand, an evident disagreement between the theoretical and experimental TO branches still exists along the Γ-X-K path, regardless of the localization/delocalization (values of U) of the 5f states and the presence/absence of spin-orbit coupling. To explain this feature we have considered intensities of the phonon modes provided by the $F(\mathbf{k}, j)$ factor defined by Eq. (1). It occurs that the problematic TO branch along the Γ-X-K path exhibits $F(\mathbf{k}, j) \to 0$, and hence negligible intensity in comparison with the remaining acoustic and optical branches. This clarifies why the Γ-X-K transverse optic branch was hardly detected in the INS experiments [19]. We also note that this branch carries very low intensity independently of the values of the Hubbard term U and the presence or absence of SOI.

One concludes that in contrast to the dynamics of uranium atoms, vibrations of the carbon atoms in UC remain much more sensitive to the changes in charge redistribution induced by the partial localization of the 5f electrons and spin-orbit coupling, which substantially affect the interatomic force constants and hence the optical phonon frequencies. A similar effect has already been observed in other actinide materials [34,36].

Finally, we discuss the phonon densities of states calculated within the DFT+U+SO approach with $U = 2$ eV which are displayed in Fig. 7(a). We also compare the resulting

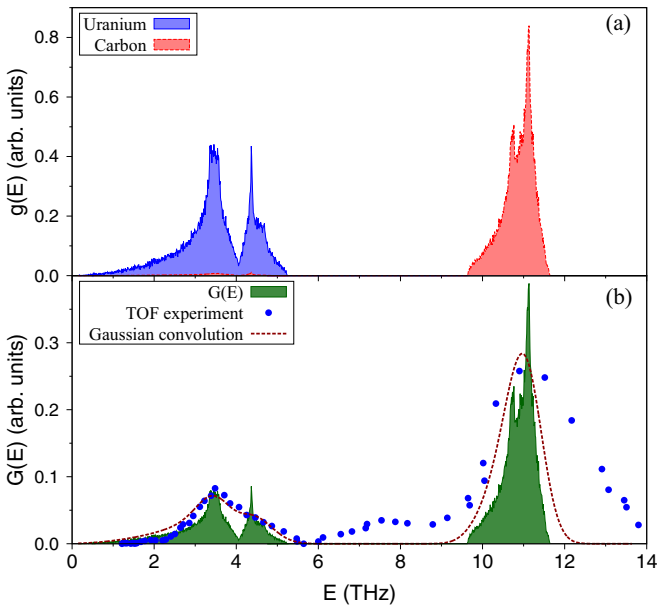

FIG. 7. (a) Partial phonon densities of states $g(E)$ for uranium and carbon atoms in UC. (b) Generalized phonon density of states $G(E)$ in UC. The TOF data (solid symbols) are taken from Ref. [25]. Simulations are performed within the DFT+U+SO scheme at $U = 2$ eV. Dashed curves represent the Gaussian convolutions of our theoretical results with the hypothetical experimental resolution of 0.8 THz.

phonon spectra to those measured by the time-of-flight (TOF) technique and reported by Wedgwood [25]; see Fig. 7(b). The partial densities of phonon states indicate that the low- and high-frequency bands in UC are separated by a gap of about 5 THz and involve practically pure vibrations of the U and C sublattices, respectively. The low-frequency phonon band shows a two-peak pattern whereas the peaks of the high-frequency band remain hardly resolved.

In order to directly compare theoretical and the INS experimental phonon spectra one needs to evaluate the neutron-weighted partial phonon densities states since the measured scattering function is sensitive to the different scattering efficiencies, σ_μ/M_μ, of the atomic species constituting particular sublattices of the investigated system [40]. Hence, the resulting generalized density of phonon states $G(E)$ is usually distinct from the *bare* phonon density of states. Due to the neutron scattering efficiencies of the uranium (0.037 barns/amu) and carbon (0.462 barns/amu) atoms [42], the uranium and carbon sublattices contribute respectively 7.4% and 92.6% to the generalized phonon density of states. Such a small contribution from uranium sublattice accounts for the diminished intensities of the phonon peaks in the low-frequency range, as can be seen in Fig. 7(b). In this range of frequencies we find very close correspondence between the calculated and experimental spectra. On the other hand, the high-frequency band determined from the INS experiments shows a broader distribution and extends to higher frequencies than the band predicted theoretically. Furthermore, in the experimental spectrum the low-intensity broad band emerges between 6 THz and 9 THz. These features of the INS spectrum, which are absent in the theoretical one, might be associated with additional atomic vibrations due to some defects existing in the measured sample. Indeed, the examined specimens contained from 1 at. % ($UC_{0.98}O_{0.02}$) to 7 at. % ($UC_{0.86}O_{0.14}$) of oxygen impurities and 1 mole % of the UO_2 contaminating phase [25]. It should be mentioned that the room-temperature phonon spectrum of UO_2 [51] significantly differs from that of UC. First of all, it exhibits no frequency gap separating the vibrations of uranium and oxygen sublattices. In addition, it extends up to about 20 THz and shows intense peaks at ~8 THz and ~13.5 THz, i.e., in the vicinity of frequencies where the low-intensity broad band and the tail of high-frequency band are found in the experimental phonon spectrum of UC. It seems, therefore, likely that the UO_2 impurity phase is responsible for the modifications of the UC experimental phonon spectra.

Theoretical phonon density of states allows for estimation of the Debye temperature Θ_D [52]. The $\Theta_D^{\mathrm{cal}} = 305$ K is evaluated at $U = 2$ eV. On one hand, the Θ_D^{cal} closely corresponds to $\Theta_D^{\mathrm{exp}} = 304 \pm 8$ K obtained from the low-temperature heat capacity measurements performed on a high-purity sample [53], but on the other hand we note that the reported values of Θ_D^{exp} range from ~270 to ~366 K, depending on the sample composition and its preparation procedure as well as the method of measurement [17]. Our theoretical Θ_D^{cal} behaves in a nonlinear manner as a function of U and its course is similar to that shown in Fig. 4(b), with the initial and final values of 273 and 327 K for the lowest and highest limits of the applied parameters U, respectively. Due to a wide spread in the experimentally determined values of Θ_D, it is rather not feasible to establish which value of the local Coulomb interaction parameter approximates Θ_D^{exp} most accurately.

IV. SUMMARY AND CONCLUSIONS

The electronic, magnetic, elastic, and phonon properties of uranium monocarbide have been explored within density functional theory incorporating the spin-orbit and strong local interactions of the Coulomb type. Results of this research clearly show considerable role of the correlated nature of the $5f$ electrons together with SOI on the aforementioned properties of UC. The DFT+U+SO implementation with $U = 2$ eV describing the partial localization of the electronic states in the $5f$ shell allowed us to improve compatibility between the experimental and calculated electronic structure of UC. Also, both effects were found to be important for theoretical prediction of the elastic constants of this system. By combining the spin-orbit interaction with the partial localization of $5f$ electrons and treating them on equal footing one could successfully reproduce the measured phonon dispersion curves and resolve the issue about dispersionless optical branches in UC. These could not be achieved before mainly because of neglecting the spin-orbit coupling in most of the previous theoretical research. This additionally confirms that a treatment of the $5f$ electrons as fully delocalized (in the DFT scheme) or partially localized (in the DFT+U scheme) without incorporation of the SOI is insufficient for description of such actinide compounds as UC. Application of the phonon form factor appeared very useful in depicting the intensities of phonon modes and accounted for the lack of signal in the neutron scattering measurements due to the low-intensity TO phonons along the Γ-X-K path. Comparison of the calculated and experimental neutron-weighted phonon densities of states reveals the presence of contaminating phase or some defects in the measured UC sample. This suggestion may be verified by the DFT+U+SO calculations of phonon spectra for the UC lattice containing carbon vacancies or oxygen impurities.

The present DFT+U+SO approach seems promising in refining the fundamental properties of other uranium rocksalt structure compounds, such as UN, for which a combination of electron localization with the spin-orbit interaction was shown [31] to be important for proper description of its electronic and magnetic structure. It is also likely that implementation of the spin-orbit interaction together with a moderate localization of the $5f$ electrons may eliminate discrepancy between experimental [19] and the DFT-calculated [54] optical phonon modes in UN.

ACKNOWLEDGMENTS

This work was supported by the Ministry of Education, Youth, and Sports from the Large Infrastructures for Research, Experimental Development, and Innovations project IT4Innovations National Supercomputing Center LM2015070. The Interdisciplinary Center for Mathematical and Computational Modeling (ICM), Warsaw University, Poland, is acknowledged for providing computer facilities under Grant No. G28-12.

[1] C. A. Utton, F. D. Bruycker, K. Boboridis, R. J. H. Noel, C. Guéneaud, and D. Manara, J. Nucl. Mater. **385**, 443 (2009).

[2] R. Eloirdi, A. J. Fuchs, J.-C. Griveau, E. Colineau, A. B. Shick, D. Manara, and R. Caciuffo, Phys. Rev. B **87**, 214414 (2013).

[3] U. Carvajal-Nunez, L. Martel, D. Prieur, E. L. Honorato, R. Eloirdi, I. Farnan, T. Vitova, and J. Somers, Inorg. Chem. **52**, 11669 (2013); U. Carvajal-Nunez, R. Eloirdi, D. Prieur, L. Martel, E. L. Honorato, I. Farnan, T. Vitova, and J. Somers, J. Alloys Compds. **589**, 234 (2014).

[4] C. B. Basak, Comput. Mater. Sci. **40**, 562 (2007).

[5] L. Petit, A. Svane, Z. Szotek, W. M. Temmerman, and G. M. Stocks, Phys. Rev. B **80**, 045124 (2009).

[6] H. Shi, P. Zhang, S.-S. Li, B. Sun, and B. Wang, Phys. Lett. A **373**, 3577 (2009).

[7] M. Freyss, Phys. Rev. B **81**, 014101 (2010).

[8] H. Shi, P. Zhang, S.-S. Li, B. Wang, and B. Sun, J. Nucl. Mater. **396**, 218 (2010).

[9] R. Ducher, R. Dubourg, M. Barrachin, and A. Pasturel, Phys. Rev. B **83**, 104107 (2011).

[10] Q. Yin, A. Kutepov, K. Haule, G. Kotliar, S. Y. Savrasov, and W. E. Pickett, Phys. Rev. B **84**, 195111 (2011).

[11] X.-D. Wen, S. P. Rudin, E. R. Batista, D. L. Clark, G. E. Scuseria, and R. L. Martin, Inorg. Chem. **51**, 12650 (2012).

[12] X.-D. Wen, R. L. Martin, G. E. Scuseria, S. P. Rudin, and E. R. Batista, J. Phys. Chem. C **117**, 13122 (2013).

[13] B. Sahoo, K. Joshi, and S. C. Gupta, J. Nucl. Mater. **437**, 81 (2013).

[14] D. Butler, Nature (London) **429**, 238 (2004); D. Petti, D. Crawford, and N. Chauvin, MRS Bull. **34**, 40 (2009).

[15] M. K. Meyer, R. Fielding, and J. Gan, J. Nucl. Mater. **371**, 281 (2007); D. C. Crawford, D. L. Porter, and S. L. Hayes, *ibid.* **371**, 202 (2007).

[16] H. Matsui, M. Horiki, and T. Kirihara, J. Nucl. Sci. Technol. **18**, 922 (1981); F. L. Guyadec, C. Rado, S. Joffre, S. Coullomb, C. Chatillon, and E. Blanquet, J. Nucl. Mater. **393**, 333 (2009).

[17] H. Holleck and H. Kleykamp, in *Gmelin Handbook of Inorganic Chemistry*, 8th ed., edited by R. Keim and C. Keller (Springer-Verlag, Berlin, 1986), Vol. C 12.

[18] E. K. Storms, *The Refractory Carbides* (Academic Press, New York, 1967), and references therein .

[19] J. A. Jackman, T. M. Holden, W. J. L. Buyers, P. de V. DuPlessis, O. Vogt, and J. Genossar, Phys. Rev. B **33**, 7144 (1986).

[20] P. Maldonado, L. Paolasini, P. M. Oppeneer, T. R. Forrest, A. Prodi, N. Magnani, A. Bosak, G. H. Lander, and R. Caciuffo, Phys. Rev. B **93**, 144301 (2016).

[21] J. W. L. Pang, W. J. L. Buyers, A. Chernatynskiy, M. D. Lumsden, B. C. Larson, and S. R. Phillpot, Phys. Rev. Lett. **110**, 157401 (2013).

[22] J. Trygg, J. M. Wills, M. S. S. Brooks, B. Johansson, and O. Eriksson, Phys. Rev. B **52**, 2496 (1995).

[23] B. Dorado and P. Garcia, Phys. Rev. B **87**, 195139 (2013).

[24] T. Ejima, K. Murata, S. Suzuki, T. Takahashi, S. Sato, T. Kasuya, Y. Onuki, H. Yamagami, A. Hasegawa, and T. Ishii, Physica B **186-188**, 77 (1993).

[25] F. A. Wedgwood, J. Phys. C: Solid State Phys. **7**, 3203 (1974).

[26] G. Kresse and J. Furthmüller, Phys. Rev. B **54**, 11169 (1996); Comput. Mater. Sci. **6**, 15 (1996).

[27] J. P. Perdew, K. Burke, and M. Ernzerhof, Phys. Rev. Lett. **77**, 3865 (1996); **78**, 1396 (1997).

[28] S. L. Dudarev, G. A. Botton, S. Y. Savrasov, C. J. Humphreys, and A. P. Sutton, Phys. Rev. B **57**, 1505 (1998).

[29] S. L. Dudarev, D. N. Manh, and A. P. Sutton, Philos. Mag. B **75**, 613 (1997).

[30] D. van der Marel and G. A. Sawatzky, Phys. Rev. B **37**, 10674 (1988).

[31] D. Gryaznov, E. Heifets, and E. Kotomin, Phys. Chem. Chem. Phys. **14**, 4482 (2012).

[32] M. Gajdoŝ, K. Hummer, G. Kresse, J. Furthmüller, and F. Bechstedt, Phys. Rev. B **73**, 045112 (2006).

[33] K. Parlinski, Z.-Q. Li, and Y. Kawazoe, Phys. Rev. Lett. **78**, 4063 (1997); K. Parlinski, Software PHONON, ver. 6.15, Kraków, Poland, 2015.

[34] P. Piekarz, K. Parlinski, P. T. Jochym, A. M. Oleś, J.-P. Sanchez, and J. Rebizant, Phys. Rev. B **72**, 014521 (2005).

[35] Y. Yun, D. Legut, and P. Oppeneer, J. Nucl. Mater. **426**, 109 (2012); G. Kaur, P. Panigrahi, and M. C. Valsakumar, Modell. Simul. Mater. Sci. Eng. **21**, 065014 (2013).

[36] S. Raymond, P. Piekarz, J.-P. Sanchez, J. Serrano, M. Krisch, B. Janoušová, J. Rebizant, N. Metoki, N. K. Kaneko, P. Jochym, A. Oleś, and K. Parlinski, Phys. Rev. Lett. **96**, 237003 (2006).

[37] N. Metoki, K. Kaneko, S. Raymond, J.-P. Sanchez, P. Piekarz, K. Parlinski, A. M. Oleś, S. Ikeda, T. D. Matsuda, Y. Haga, Y. Anuki, and G. H. Lander, Phys. B (Amsterdam, Neth.) **378-380**, 1003 (2006); J. Buhot, M. A. Méasson, Y. Gallais, M. Cazayous, A. Sacuto, F. Bourdarot, S. Raymond, G. Lapertot, D. Aoki, L. P. Regnault, A. Ivanov, P. Piekarz, K. Parlinski, D. Legut, C. C. Homes, P. Lejay, and R. P. S. M. Lobo, Phys. Rev. B **91**, 035129 (2015).

[38] A. Sjölander, Ark. Fys. **14**, 315 (1958).

[39] U. D. Wdowik and K. Parlinski, Phys. Rev. B **78**, 224114 (2008); J. Phys.: Condens. Matter **21**, 125601 (2009).

[40] S. W. Lovesey, *Theory of Neutron Scattering from Condensed Matter* (Oxford University Press, Oxford, 1987), Chap. 4.

[41] U. D. Wdowik, K. Parlinski, T. Chatterji, S. Rols, and H. Schober, Phys. Rev. B **82**, 104301 (2010).

[42] V. F. Sears, Neutron News **3**, 26 (1992); A. J. Dianoux and G. Lander, eds., *Neutron Data Booklet* (Institut Laue-Langevin, Grenoble, France, 2002).

[43] U. D. Wdowik and D. Legut, J. Phys.: Condens. Matter **21**, 275402 (2009); U. D. Wdowik, P. Piekarz, K. Parlinski, A. M. Oleś, and J. Korecki, Phys. Rev. B **87**, 121106(R) (2013); U. D. Wdowik, P. Piekarz, P. T. Jochym, K. Parlinski, and A. M. Oleś, *ibid.* **91**, 195111 (2015).

[44] P. Söderlind, G. Kotliar, K. Haule, P. Oppeneer, and D. Guillaumont, MRS Bull. **35**, 883 (2010).

[45] E. K. Storms and E. J. Huber, J. Nucl. Mater. **23**, 19 (1967).

[46] J. Williams, R. A. J. Sambell, and D. Wilkinson, J. Less-Common Met. **2**, 352 (1960).

[47] W. J. L. Buyers and T. M. Holden, in *Handbook on the Physics and Chemistry of the Actinides*, edited by A. Freeman and G. Lander (North Holland, Amsterdam, 1985), Vol. 2, p. 239 .

[48] J. L. Routbort, J. Nucl. Mater. **40**, 17 (1971).

[49] W. G. Stirling, G. H. Lander, and O. Vogt, J. Phys. C **16**, 4093 (1983).

[50] P. de V. DuPlessis, T. M. Holden, W. J. L. Buyers, J. A. Jackman, A. F. Murray, and C. F. V. Doom, J. Phys. C **18**, 2809 (1985).

[51] J. Pang, A. Chernatynskiy, B. Larson, W. J. L. Buyers, D. L. Abernathy, K. J. McClellan, and S. Phillpot, Phys. Rev. B **89**, 115132 (2014).

[52] G. Grimvall, *Thermophysical Properties of Materials* (Elsevier, North-Holland, Amsterdam, 1999).

[53] E. Westrum, Y. Takahashi, and N. D. Stout, J. Phys. Chem. **69**, 1520 (1965).

[54] P. Modak and A. K. Verma, Phys. Rev. B **84**, 024108 (2011).